Geophysical Research Letters

RESEARCH LETTER
10.1029/2024GL112200

Dissociating Gas Hydrate Beneath the Hydrate Stability Zone

I. A. Pecher[1,2], A. E. Cook[3], E. A. Solomon[4], X. Wang[5], S. Han[6], M. Paganoni[7,8], M. Luo[9], K. U. Heeschen[10], D. D. McNamara[11], M. Nole[12,13], L. LeVay[14], K. Petronotis[14], P. M. Barnes[15], L. M. Wallace[6,16], and D. M. Saffer[6]

[1]Texas A&M University – Corpus Christi, Corpus Christi, TX, USA, [2]University of Auckland, Auckland, New Zealand, [3]Ohio State University, Columbus, OH, USA, [4]University of Washington, Seattle, WA, USA, [5]Key Lab of Submarine Geosciences and Prospecting Techniques, Ocean University of China, Qingdao, China, [6]University of Texas Institute for Geophysics, Austin, TX, USA, [7]Now at Snam, Business Unit Asset Italia Storage, San Donato Milanese, Italy, [8]Oxford University, Oxford, UK, [9]Shanghai Ocean University, Shanghai, China, [10]GeoForschungsZentrum Potsdam, Potsdam, Germany, [11]University of Liverpool, Liverpool, UK, [12]Now at ResFrac Corporation, Denver, CO, USA, [13]Pacific Northwest National Laboratory, Richland, WA, USA, [14]Texas A&M University, College Station, TX, USA, [15]National Institute of Water and Atmospheric Research, Wellington, New Zealand, [16]GEOMAR Helmholtz Centre for Ocean Research, Kiel, Germany

Abstract Vast amounts of carbon are stored beneath the seafloor in the form of methane hydrate. Hydrate is stable at moderate pressure and low temperature at a depth extending several hundred meters beneath the seafloor to the base of gas hydrate stability (BGHS) often marked by bottom simulating reflections (BSRs) in seismic profiles. However, data from logging-while-drilling and coring during Integrated Ocean Discovery Program Expeditions 372 and 375 offshore New Zealand identified hydrate ~60 m beneath the BSR. This hydrate appears to be dissociating over thousands of years following a gradual temperature increase from sediment burial modulated by changes in bottom-water temperature and sea-level fluctuations. Slow hydrate dissociation significantly buffers the release of methane and therefore, carbon through glacial cycles. Dissociating hydrate beneath the BGHS may also increase estimated global budgets of methane stored in hydrate.

Plain Language Summary Frozen methane or methane hydrate is commonly present in sediments on continental slopes. Methane hydrate occurs from the seafloor to several hundred meters beneath the seafloor; the base of hydrate stability is controlled by pressure, temperature, and salinity. However, hydrate was observed ~60 m below the base of stability in data collected from scientific ocean drilling offshore New Zealand. This hydrate appears to be melting over thousands of years following sediment deposition, probably also influenced by sea-level and temperature fluctuations through glacial cycles. Slow hydrate melting may buffer any release of methane from hydrates into the ocean. Melting hydrate below the base of hydrate stability, if commonly present elsewhere, may also increase estimates of the amounts of methane stored in hydrate globally.

Key Points:

- Results from borehole logging and coring show evidence for gas hydrate well beneath the regional base of gas hydrate stability
- We infer hydrate to be in an ongoing process of dissociation over thousands of years
- A release of carbon from hydrate following changes in pressure and temperature through glacial cycles may be strongly buffered

Supporting Information:

Supporting Information may be found in the online version of this article.

Correspondence to:

I. A. Pecher,
ingo.pecher@tamucc.edu

Citation:

Pecher, I. A., Cook, A. E., Solomon, E. A., Wang, X., Han, S., Paganoni, M., et al. (2025). Dissociating gas hydrate beneath the hydrate stability zone. *Geophysical Research Letters*, *52*, e2024GL112200. https://doi.org/10.1029/2024GL112200

Received 30 AUG 2024
Accepted 12 MAY 2025

Author Contributions:

Conceptualization: I. A. Pecher, A. E. Cook, E. A. Solomon, X. Wang, S. Han, M. Paganoni, M. Luo, K. U. Heeschen, D. D. McNamara, M. Nole, P. M. Barnes, L. M. Wallace, D. M. Saffer
Formal analysis: I. A. Pecher, A. E. Cook, E. A. Solomon, X. Wang, M. Luo
Funding acquisition: I. A. Pecher, A. E. Cook, E. A. Solomon, X. Wang, P. M. Barnes, L. M. Wallace, D. M. Saffer
Investigation: I. A. Pecher, A. E. Cook, E. A. Solomon, X. Wang, S. Han, M. Paganoni, M. Luo, K. U. Heeschen, D. D. McNamara, P. M. Barnes, L. M. Wallace, D. M. Saffer

1. Introduction

Methane hydrate is an ice-like substance containing methane and water and is commonly present at moderate pressures and low temperatures beneath the seafloor on continental slopes. Because of the geothermal gradient, hydrate is only stable to the base of gas hydrate stability (BGHS), usually a few hundred meters below the seafloor. Free gas may be present at the BGHS, causing bottom simulating reflections (BSRs) in seismic data that are sub-parallel to the seafloor. The thickness of the free-gas zone (FGZ) beneath BSRs has been found to range from less than a few meters (Bangs et al., 1993; I. A. Pecher et al., 1996; Singh et al., 1993) to 500–600 m (A. M. Tréhu & Flueh, 2001).

Methane hydrate sequesters on the order of ~10^2–10^3 Gt of carbon, comprising 5%–25% of Earth's mobile exogenic carbon (Buffett & Archer, 2004; Dickens, 2003; Milkov et al., 2003; Ruppel, 2011; Wallmann et al., 2012). A bottom-water temperature increase or sea-level decrease, including from tectonic uplift, may destabilize submarine hydrate releasing some of this carbon (Kennett et al., 2000; Oluwunmi et al., 2022). Methane from hydrate dissociation may be bound as near-seafloor carbonate but if released into the ocean, it is expected to be oxidized to CO_2 and potentially contribute to ocean acidification of marginal seas (Biastoch

Methodology: I. A. Pecher, A. E. Cook, E. A. Solomon, X. Wang, S. Han, M. Paganoni, M. Luo, K. U. Heeschen, D. D. McNamara, M. Nole, P. M. Barnes, L. M. Wallace, D. M. Saffer
Project administration: I. A. Pecher, L. LeVay, K. Petronotis, P. M. Barnes, L. M. Wallace, D. M. Saffer
Resources: I. A. Pecher, A. E. Cook, L. LeVay, K. Petronotis
Software: I. A. Pecher, A. E. Cook
Validation: I. A. Pecher, A. E. Cook, E. A. Solomon, X. Wang, M. Luo
Visualization: I. A. Pecher, A. E. Cook, E. A. Solomon
Writing – original draft: I. A. Pecher, A. E. Cook, E. A. Solomon, X. Wang, S. Han, M. Luo, K. U. Heeschen, D. D. McNamara, M. Nole, L. LeVay, K. Petronotis, P. M. Barnes, L. M. Wallace, D. M. Saffer
Writing – review & editing: M. Paganoni

et al., 2011). Dissociation of solid hydrate to water and pressurized gas may also destabilize the seafloor (Maslin et al., 2010).

Constraining the timescales for the dissociation of hydrate in response to pressure and temperature changes is critical for understanding how this carbon capacitor will buffer the release and uptake of carbon through glacial cycles and, potentially, in response to human-induced climate change (Dickens, 2003; Kennett et al., 2000). It is often implicitly assumed that the time required for hydrate systems to respond to perturbations is short relative to geologic processes. This assumption may be based on the observed fast dissociation of hydrates in relatively small sediment samples following a sudden pressure drop during core recovery or in the laboratory.

Recent modeling, however, suggests hydrate dissociation in sub-seafloor sediments may take thousands of years. Goto et al. (2016) modeled the thermal effects of hydrate dissociation during repeated tectonic uplift by considering endothermic dissociation a heat sink. Temperatures were arrested at the hydrate phase boundary until they had fully dissociated. Depending on uplift rates, it took ~6,000 to ~40,000 years for a 10-m thick layer with a hydrate saturation of 60% to fully dissociate. Models of hydrate dissociation in porous media that include multiphase fluid migration show that in addition to endothermic cooling, slow dissipation of pressure and salinity slow down hydrate dissociation during uplift even further (Oluwunmi et al., 2022). Pore-scale models of hydrate dissociation following burial predict co-existence of hydrate with gas over extended times (Nole et al., 2018; You & Flemings, 2021). Because of capillary forces, hydrate stability decreases with decreasing pore size and thus, dissociation during burial is predicted to progress from smaller to larger pores. This results in a three-phase zone with water and free gas in smaller and hydrate in larger pores that may be tens of meters thick, equivalent to thousands to tens of thousands of years of burial.

Herein, we provide observational evidence for such slow hydrate dissociation within a thick FGZ beneath a BSR. Our observations are from downhole logs and cores from International Ocean Discovery Program (IODP) Site U1519 on the Hikurangi Margin east of New Zealand's North Island (Figure 1). On this margin, the Pacific Plate is being subducted beneath the Australian Plate at ~45 mm/yr (DeMets et al., 1990). Gas hydrate is widespread along this margin as indicated by BSRs (I. A. Pecher & Henrys, 2003). Gas for hydrate formation was found to be almost entirely microbial with the exception of limited thermogenic input near the southern end of the margin (Kroeger et al., 2015). At several locations along this margin, double BSRs have been identified, with the deeper BSRs marking a paleo-position of the BGHS, thus indicating past changes in pressure-temperature conditions resulting from tectonic uplift or burial (Han et al., 2021; I. A. Pecher et al., 2017).

2. Data

2.1. Seismic Data and IODP Expeditions

Seismic line 05CM-04 was acquired in 2005 by the New Zealand Government's Crown Minerals to encourage exploration of marine resources (Multiwave, 2005) (Figure 1a). IODP Expeditions 372 and 375 in 2017 and 2018 collected logging-while-drilling (LWD) data and sediment cores at Site U1519 (Wallace et al., 2019) positioned on Line 05CM-04 to reveal a broad suite of petrophysical and lithological properties.

2.2. Logging and Coring

Forty meters of Schlumberger LWD tools were attached behind the bit and collected measurements during drilling of Hole U1519B. Sediment cores were retrieved later at selected intervals in a separate Hole U1519C, ~20 m to the east-south-east (Barnes et al., 2019).

Natural gamma-ray intensity, measured in API (American Petroleum Institute) units, was used to distinguish qualitatively between clay- (high intensity) and quartz-rich sediments. Neutron porosity has been measured based on the amount of hydrogen in formations (Ellis & Singer, 2007). Ring resistivity, based on a radial flow of current into the formation, was selected from the various resistivity measurements because it has the best-suited vertical resolution (~5–8 cm) (Barnes et al., 2019). P- and S-wave velocities were measured using a monopole and a quadrupole source, respectively, at frequencies of 1–20 kHz yielding a vertical resolution of ~10 cm. Velocities were determined at the Lamont Doherty Earth Observatory using Leaky P and Leaky Q processing (Saumya et al., 2019). Pore-water chemistry, in particular, chlorinity, $\delta^{18}O$ and δD (see below) was measured on sediment cores.

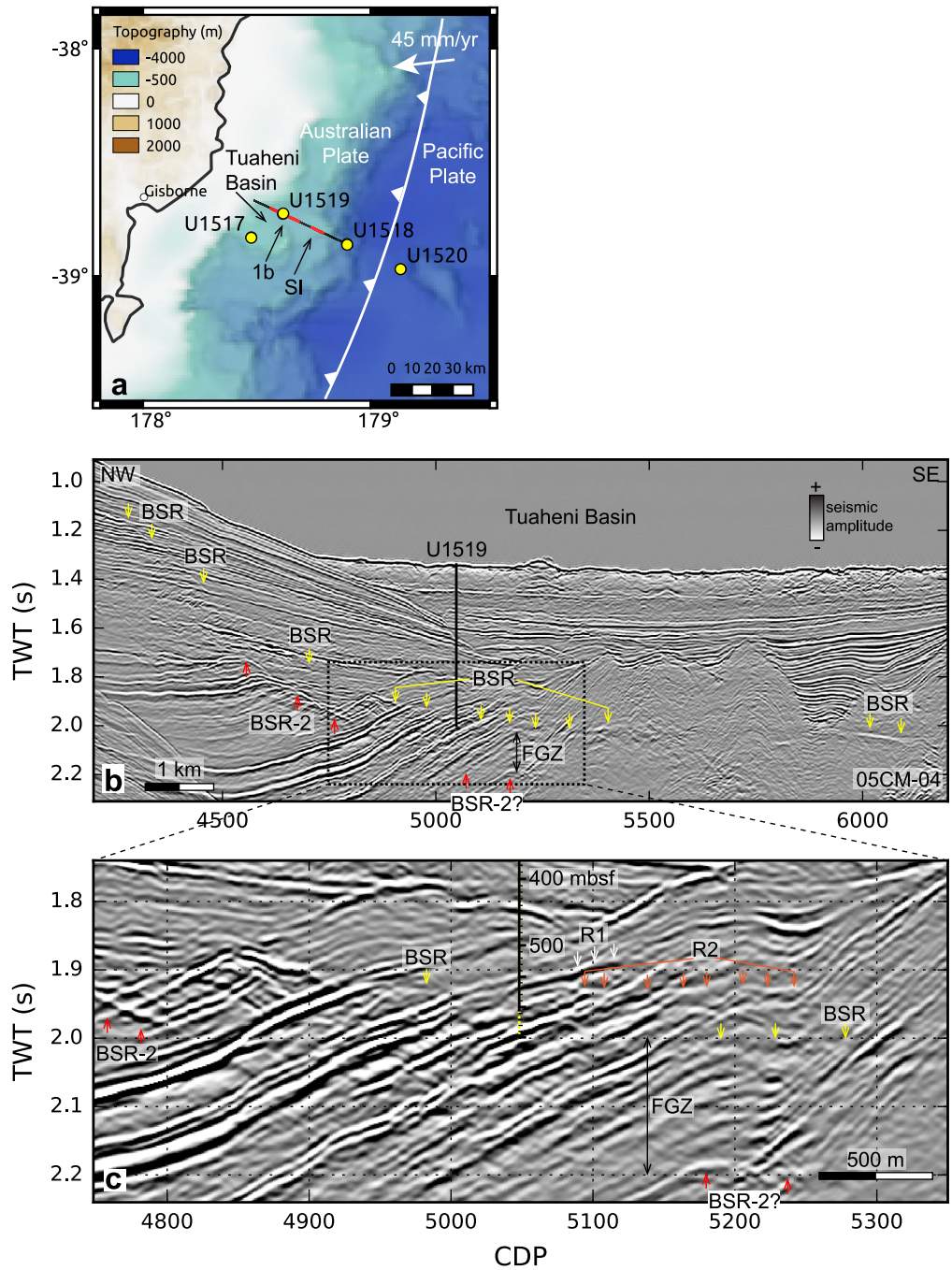

Figure 1. (a) Location map with seismic data track. Plate convergence vector after DeMets et al. (1990). Red segments shown in panel (b) and Figure S7 in Supporting Information S1. See Text S1 for log-seismic ties. (b) Seismic line 05CM-04, processed for high resolution (Navalpakam et al., 2012). BSR-2 interpreted as paleo-BSR (Han et al., 2021). (c) Enlargement at Site U1519. Yellow-dashed part at the bottom of the borehole marks 40-m long tool string above the deepest position of the drill bit. This interval was not logged with all tools ("rat hole"). R1: Gas-bearing sand, R2: Newly forming BSR, see text and Figure 3g.

3. Methods

Gas hydrate saturation was constrained from resistivity, velocities, and chlorinity (Cl).

3.1. Resistivity

Hydrate saturation was calculated from resistivity using Archie's Equation (Cook & Waite, 2018) based on neutron porosity ϕ. Pore-water resistivity was assumed to be 0.24 Ωm (Shkvorets, 2025) for a salinity of 3.3%, a temperature of 15.7°C, and hydrostatic pressure at 540 mbsf. This depth is in the interval from 492 to 563 mbsf that was used to calibrate the resistivity of fully water-saturated (hydrate-free) sediments (Table S1 in Supporting Information S1) yielding a cementation exponent of $m = 2.76$ (Text S2, Figure 2, Figure S3 in Supporting Information S1). An Archie saturation exponent of $n = 2.5$ (Cook & Waite, 2018) with an n range of ±0.5 was used for calculating hydrate saturation. This range does not affect our interpretation of hydrate-bearing intervals, only the saturation in these intervals (Text S3 in Supporting Information S1).

3.2. P- and S-Wave Velocities

An empirical approach, the modified Biot-Gassmann Theory by Lee (BGTL) (Lee, 2002, 2008; Lee & Collet, 2005), was used to constrain hydrate saturation from velocities. Properties of the solid material are calculated using the Hill average (Hill, 1952) of the mineral constituents with a composition based on shipboard X-Ray Diffraction analyses (Wallace et al., 2019). Effective pressure, that is, the difference between lithostatic and hydrostatic pressure, is calculated using neutron density.

We defined a porosity-velocity relationship using V_p, V_s, and ϕ in the hydrate-free reference section between 492 and 563 m. In this interval, we calibrated the Biot-h factor as $h = 0.98$ and the Biot-m factor as $m = 3.0$. It then is possible to predict V_p and V_s as a function of porosity and differential pressure. V_p and V_s of hydrate-bearing sediments are then predicted by including hydrate as a part of the modal assemblage in the Hill average, reducing porosity accordingly. The weight percentage of mineral constituents are averages over the coring interval beneath 520 mbsf consisting of clays (44.6%), quartz (25.9%), feldspar (15.7%), and calcite (13.8%) (Wallace et al., 2019). Values from the literature were used for density and elastic moduli (Helgerud et al., 1999, 2009; Mavko et al., 2020; Pabst & Gregorová, 2013). Density from clay minerals in the literature is highly variable. Here, it was modified such that grain density of all mineral phases combined matched that measured on cores in the interval >520 mbsf (2,667 kg/m^3) (Wallace et al., 2019) yielding 2,680 kg/m^3. Refer to Text S4 and Table S2 in Supporting Information S1 for further details.

3.3. Chlorinity

Hydrate excludes ions during formation and thus, hydrate dissociation during core recovery releases fresh water decreasing chlorinity. Hydrate is furthermore enriched in ^{18}O and ^{2}H (Deuterium: D) isotopes leading to an enrichment in δ^{18}O and δD in pore water during dissociation (Kastner et al., 1991; Ussler & Paull, 1995).

Chloride concentrations were measured in sediment cores shipboard via titration with silver nitrate with an analytical precision better than 0.3%. Oxygen and hydrogen isotope ratios were measured using a Picarro L2130-i cavity ringdown spectrometer at the University of Washington. Uncertainties in the δ^{18}O and δD measurements are 0.07 and 0.2‰, respectively.

Background chlorinity, determined as average chlorinity in the hydrate-free interval of 492–563 mbsf, outside the interval of a long-wavelength Cl-excursion (Figure 2b), was 525.3 mM, slightly less than standard seawater (559 mM) (Text S5 in Supporting Information S1). Hydrate saturation was calculated from Cl-excursions from the background chlorinity (Malinverno et al., 2008). The average δ^{18}O and δD isotope ratios are also lower than for seawater, −1.6‰ and −1.9‰, respectively, and were investigated qualitatively.

3.4. Temperature

Subseafloor temperatures were constrained using a bottom-water temperature of 5.6°C from CTD data (Mountjoy et al., 2014), BSR depth (581 mbsf, see below), and assuming methane hydrate in seawater (Sloan & Koh, 2007), resulting in a predicted geothermal gradient of 0.0181 K/m.

4. Results and Interpretation

In seismic data, the BSR at Site U1519 is a weak, near-horizontal reflection at ~580 mbsf that marks the upper termination of dipping high-amplitude reflections (Figures 1b and 1c) and aligns with BSRs elsewhere in the

10.1029/2024GL112200

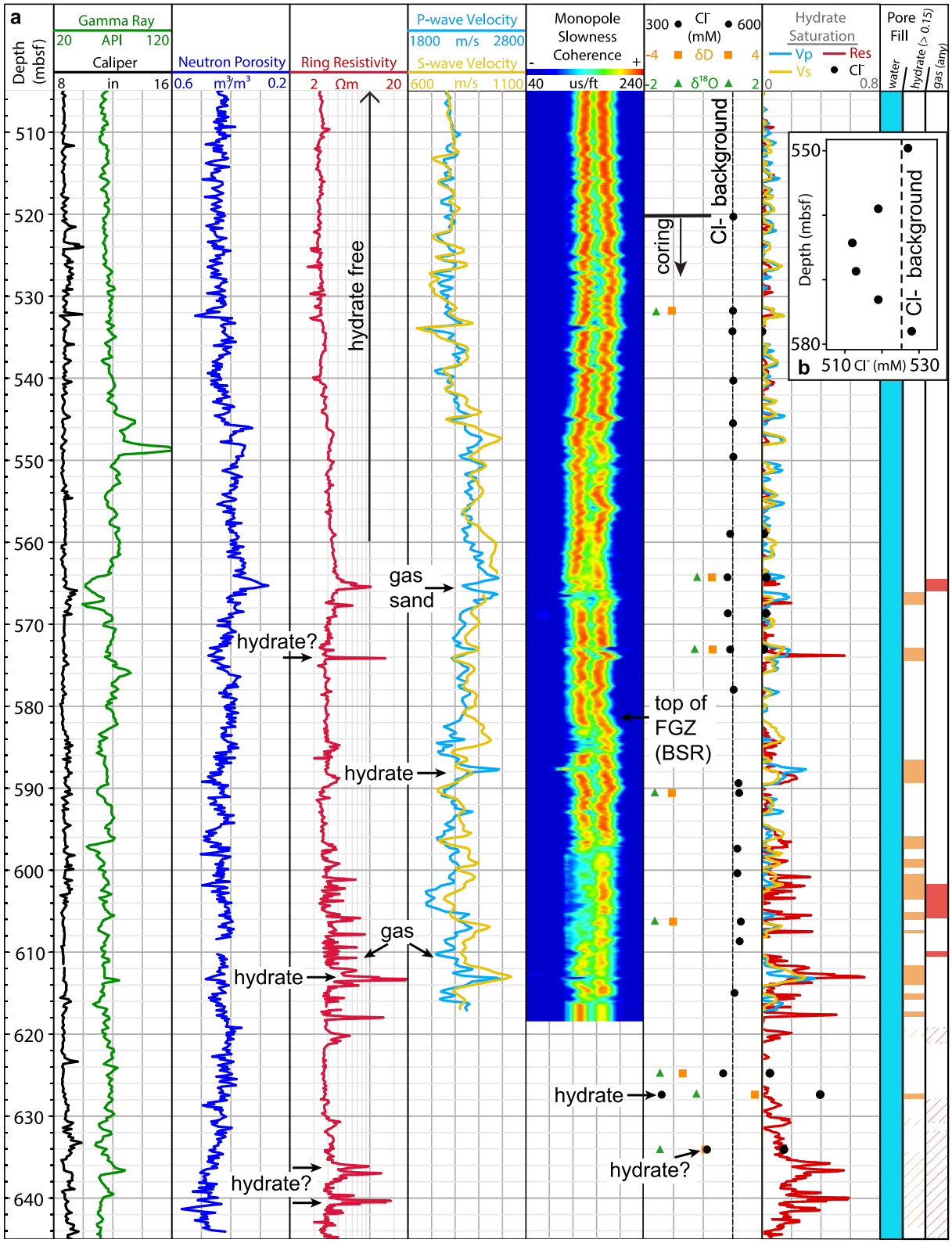

Figure 2. (a) Key logs and pore-water profiles with hydrate and gas interpretation between 505 and 645 mbsf. Coring for this depth interval was only conducted at depths >520 mbsf. Hydrate-free sediments are interpreted from smooth resistivity and sonic profiles. Gas-bearing layers are expected to be marked by elevated resistivity and lower V_p, hydrate-bearing layers by elevated resistivity and sonic velocities, lower Cl and higher $\delta^{18}O$ and δD. The BSR in the seismic data coincides with the top of free gas interpreted from a decrease in slowness coherence and V_p. (b) Enlarged Cl-profile between 550 and 580 mbsf (see text).

study region (Han et al., 2021; Navalpakam et al., 2012). A ~200 m thick zone of high amplitudes beneath the BSR is interpreted as a thick FGZ. Near the base of the FGZ at ~780 mbsf, a second BSR (BSR-2, Figures 1b and 1c) is interpreted as a paleo-BSR from gas remaining at a previous position of the BGHS (Han et al., 2021). Individual high-amplitude layers extend well below the FGZ and are interpreted as being gas-charged similar to sub-BSR high-amplitude reflections elsewhere (Navalpakam et al., 2012).

In the LWD data, the 563–567 mbsf interval beneath the hydrate-free reference section shows a decrease of porosity, gamma ray, V_p, and coherence, a loss of the S-wave signal, and an increase of resistivity (Figure 2). This is the typical signature for gas-bearing sands. Because of its lower density, free gas contains fewer hydrogen atoms per volume than water. Therefore, the decrease in neutron-porosity readings may partly reflect the presence of gas rather than an actual porosity decrease. Below this interval, from 567 to 581 mbsf, sediments are water-saturated with thin layers of hydrate (e.g., at 574 mbsf). At 581 mbsf, we interpret a lowering of coherence indicating signal degradation of P-waveforms and a long-wavelength decrease of V_p as the top of the FGZ and depth of the BSR (Figures 1 and 2).

Between 559 and 573 mbsf, four sediment cores from Hole U1519C display slightly decreased Cl values of 512–519 mM (Figure 2b). $\delta^{18}O$ and δD were measured in two of these cores and were found to be slightly elevated. A decrease of Cl combined with an increase of $\delta^{18}O$ and δD suggests hydrate dissociation. The smoothness of the Cl profiles, unlike the spikes typical of dissociation during core recovery, suggests hydrate dissociation has occurred in situ, rather than during core recovery, with sufficient time elapsed such that any discrete Cl anomalies are smoothed by diffusion (Text S5 in Supporting Information S1). We therefore suggest in this depth interval, above the regional BSR, gas hydrate is dissociating.

Within the FGZ below the BSR, we observe indications of hydrate at 588 mbsf with elevated V_p, V_s, and resistivity. Between 592 and 612 mbsf, less pronounced increases in V_p, V_s, and resistivity may also indicate hydrate, whereas low V_p accompanied by an increase of resistivity is interpreted as free gas. At 613 mbsf, V_p, V_s, and resistivity increase significantly while porosity remains almost constant. This is a typical pattern indicating the presence of hydrate.

Below the maximum depth of the velocity logs, three significant chlorinity minima are present at 625, 628, and 634 mbsf with Cl concentrations as low as 345 mM (34% less than background) as well as an enrichment in $\delta^{18}O$ and δD of up to 1.3 and 5.6‰ above background values, respectively. The combination of a significant depletion in Cl and enrichment in $\delta^{18}O$ and δD is unequivocal evidence for the presence of hydrate. We are not aware of any other, for example, diagenetic process in this environment with such a signature. The less pronounced Cl anomaly at 634 mbsf coincides with an increase of resistivity indicative of hydrate. The absence of resistivity increases associated with the other two Cl anomalies is probably caused by the 20-m distance between logging and coring boreholes and the often heterogenous distribution of hydrate (Saumya et al., 2019). Finally, the high-resistivity interval from 636 to 642 mbsf near the bottom of the borehole is also interpreted to be caused by hydrate. The most likely alternative, a high saturation of free gas, would cause an artificial decrease in neutron porosity. Another possibility, carbonate cementation, would lead to a decrease of porosity, which the logs do not display.

5. Discussion and Conclusions

Hydrate has previously been observed below BSRs in an industry borehole offshore Borneo (Paganoni et al., 2016) and in the Pearl River Mouth Basin (Qian et al., 2018; Qin et al., 2020). Offshore of Borneo, thermogenic higher-order hydrocarbon gases led to the formation of Structure-II hydrate that is stable to higher temperatures than Structure-I methane hydrate (Paganoni et al., 2016). LWD at several sites and the second gas hydrate production test at Site GMGS6-SH02 and SHSC-4J1 in the Pearl River Basin indicated the coexistence of gas hydrate and free gas below BSRs (Kang et al., 2020). With a methane content of 97.76%, it is unclear if thermogenic gases may be involved in hydrate formation in the Pearl River Mouth Basin (Qian et al., 2018).

At Site U1519, only traces of higher-order hydrocarbon gas (ethane and propane) were detected (Barnes et al., 2019) at concentrations far too low to form Structure-II hydrate (Sloan & Koh, 2007). Therefore, hydrates in the FGZ at Site U1519 are Structure-I methane hydrate occurring below the regional base of methane hydrate stability.

We observe evidence for hydrate ~60 m beneath the regional BSR. This is near the base of the borehole and does not rule out the occurrence of hydrate even deeper. The co-existence of hydrate and free gas, combined with

evidence for in situ dissociation of hydrate above the BSR, suggests that hydrate is in the process of dissociation following an upward movement of the BGHS.

Burial will lead to such an upward movement of the BGHS by changing the near-seafloor geothermal conditions. An addition of 43 m of sediments would shift the BGHS from the deepest layer with interpreted hydrate (currently, at 640 mbsf) to the BSR level (Figure 3a). These estimates ignore compaction and assume hydrostatic pore pressure. For an average sedimentation rate of ∼1 mm/yr (Crundwell & Woodhouse, 2022), this would occur within 43,000 years, noting that sedimentation rates were highly variable. This suggests hydrate dissociation at the current depth of 640 mbsf, if caused by burial, has been ongoing for tens of thousands of years.

This upward movement of the BGHS is likely to be modulated by bottom-water temperature and hydrostatic-pressure changes from sea-level variations through glacial cycles. A decrease of in situ temperature by 0.76°C would shift the BGHS down from the current BSR to 640 mbsf (Figure 3b). The pressure drop associated with sea-level lowering of 120 m, on the other hand, shifts the BGHS up by 174 m to 407 mbsf (Figure 3c). In situ temperature would then need to be lower by 1.39°C for a BGHS at 640 mbsf (Figure 3d). To estimate the amplitude of seafloor temperature variations in order to achieve in situ temperature changes of ±0.38°C (0.76°C peak-to-trough), the skin depth of a sinusoidal temperature signal was calculated (Fowler, 2005) (Figure 3e; Text S6 in Supporting Information S1). We used a bulk thermal conductivity of 1.4 W m^{-1} K^{-1}, a porosity of 0.4 (Barnes et al., 2019), as well as specific heat capacities of 4180 J kg^{-1} K^{-1} and 1000 J kg^{-1} K^{-1} for pore water and grains, respectively (Schoen, 1996) (Table S3 in Supporting Information S1). For a period of 100,000 years, reflecting glacial cycles, the skin depth is 556 mbsf, that is, slightly shallower than the BSR. At this depth, the amplitude of seafloor temperature fluctuations decreases by 1/e, meaning, in situ temperature fluctuations of ±0.38°C around the BSR would require temperature variations at the seafloor of ∼±1.1°C, which is conceivable through glacial cycles (e.g., Waelbroeck et al., 2002) (at the skin depth, the signal is phase reversed, i.e., it is warmest at the skin depth when it is coldest at the seafloor, which we ignore here since the seafloor temperature signal is unlikely sinusoidal). The propagation of a temperature step from the seafloor to the BSR was calculated to demonstrate that slow hydrate dissociation is not predominantly caused by a time lag of this thermal signal (Fowler, 2005; Text S6 in Supporting Information S1). The highest rate of temperature change at 640 mbsf occurs after ∼6,300 years (Figure 3f), less than glacial cycles or the elapsed time since the last glacial maximum at ∼19 ka (Clark et al., 2012). This suggests that if hydrate dissociation at 640 mbsf is linked to glacial-interglacial bottom-water temperature changes, this dissociation has taken place over thousands of years.

Changes of pressure-temperature conditions around the BGHS as a function of time through glacial cycles will be an interplay between three processes: (a) Burial leads to a gradual upward shift of the BGHS with respect to given sub-seafloor layers (Figure 3a). (b) Bottom-water warming after glacial maxima results in an upward movement of the BGHS (Figure 3b), but with a significant delay (Figure 3f). (c) Pressure changes from sea-level fluctuations are thought to be transmitted near-instantaneously through the sediment column. In combination, it is therefore likely that the BGHS will initially move downwards with respect to the sediment column at the last glacial termination by 54 m (Figure 3c) over the ∼8,000 years (6.75 mm/yr) during which sea-level rose by ∼120 m (Lambeck et al., 2014). This signal will be counteracted by an initially slow upward migration following bottom-water warming reaching a maximum rate of upward movement ∼6,300 years after the onset of a temperature increase at the seafloor (Figure 3f). Bottom-water temperatures need to increase by more than 1.39°C in order to offset the downward movement of the BGHS from sea-level rise (Figure 3d). While temperature changes of this order are common globally (Waelbroeck et al., 2002), a reconstruction of benthic paleo-water temperatures in the study area is still the subject of on-going analyses. These signals are superimposed on a gradual upward movement of the BGHS at the rate of burial of ∼1 mm/yr, under the simplified assumption of a constant sedimentation rate. The lack of a time series for bottom-water temperatures precludes any further thermal modeling of the movement of the BGHS as a function of time. The considerations above ignore hydrate formation and dissociation, which will arrest local pressure-temperature-salinity conditions at the phase boundary until hydrate has entirely formed or dissociated.

In summary, our estimates show that burial as well as sea-level and bottom-water temperature fluctuations may contribute to a movement of the BGHS at similar, glacial timescales. Glacial processes will thus modulate the overall upward movement of the BGHS with respect to the sediment column from burial leading to hydrate dissociation that has been ongoing for thousands to tens of thousands of years.

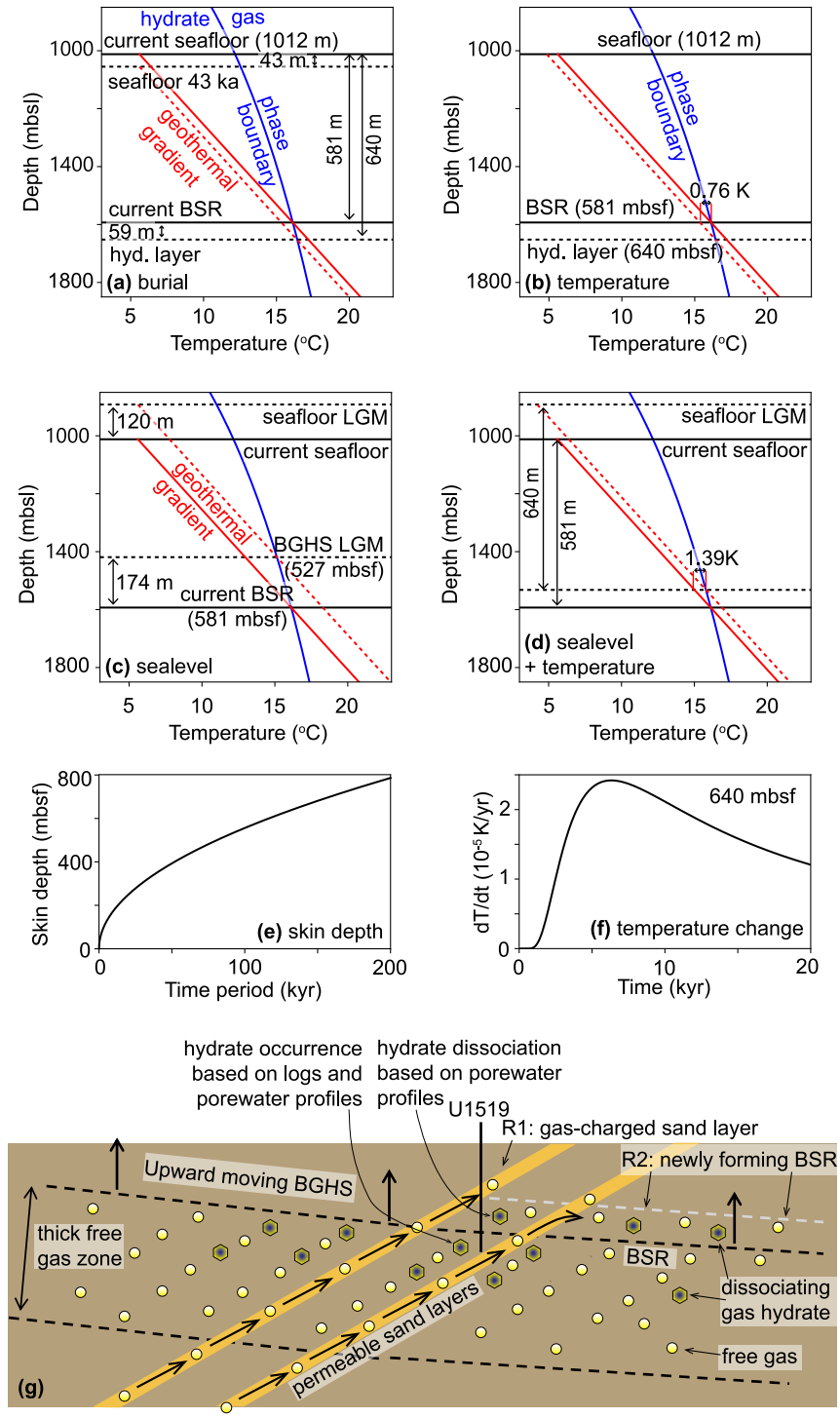

Figure 3. (a–d) Shift of predicted BGHS following burial (a), in situ temperature changes (b), sea-level lowering (c), and combined sea-level lowering and temperature changes (d). hyd. layer: Hydrate-bearing layer at 640 mbsf. mbsl: Meters beneath sea-level. Assuming hydrostatic pressure (see text for details). (e) Skin depth as a function of period of a sinusoidal temperature signal at the seafloor. For glacial cycles of ~100,000 years, the skin depth is 556 mbsf. (f) Temperature change per time as a function of time at 640 mbsf following a stepwise increase of 1°C at the seafloor. The maximum temperature change occurs after ~6,300 years. (g) Conceptual model of the adjustment of the gas hydrate system to an upward movement of the BGHS due to burial. R1, R2: Reflections labeled in Figure 1. Slowly dissociating hydrates are present beneath the BSR. Hydrate dissociation has started above the current BSR where a new BSR is being formed. Highly permeable sand layers may transport gas across the current BSR.

Hydrate in layers that are crossed by the upward migrating BGHS dissociates to water and free gas, which may then migrate upward to the new BGHS to form hydrate, that is, hydrate recycling (Nole et al., 2018; Paull et al., 1994; You & Flemings, 2021). A weak and patchy sub-horizontal reflection (R2 in Figure 1c) at ∼560 mbsf may be a newly developing BSR (Figure 1c). Partially gas-saturated dipping high-permeability sand layers like the one identified on the logs at 567 mbsf (tied to Reflection R1 in the seismic data, Figures 1c and 3g) may facilitate gas transport upward (Liu & Flemings, 2007).

Our findings support earlier modeling studies that predict hydrate dissociation to take thousands of years because of endothermic cooling (Goto et al., 2016) and additional slow salinity and pressure dissipation (Oluwunmi et al., 2022). Our results are also compatible with pore-scale models that predict hydrate to co-exist with gas following burial (Nole et al., 2018; You & Flemings, 2021). These processes result in a significant buffer for the release of methane and thus, carbon from the hydrate "capacitor" (Dickens, 2003) through glacial cycles, and potentially following future bottom-water temperature changes (Kennett et al., 2000).

Slow hydrate dissociation resulting in low rates of methane release and thus, low methane flux, may have implications for other mechanisms that buffer methane release from hydrates into the ocean. The ability of methane to migrate as free gas through the hydrate stability zone without being "trapped" as hydrate generally increases with methane flux (A. Tréhu et al., 2004). Slowly released methane is thus more likely to be recycled into the hydrate stability zone without reaching the ocean. The formation of authigenic carbonates near the seafloor, which sequesters carbon from methane, is also affected by methane flux (Boetius & Wenzhöfer, 2013). Ocean acidification of marginal seas from methane that does reach the ocean is intuitively alleviated if methane flux rates are low compared to the exchange of water masses.

We have detected hydrate in a thick FGZ beneath the regional BSR level. Thick FGZs, typically identified by zones of high-amplitude reflections in seismic data, have been observed beneath hydrate in several locations worldwide (Crutchley et al., 2015; Holbrook et al., 1996; Portnov et al., 2019). These FGZs are distinct from "sharp" BSRs without underlying zones of high reflectivity, which are thought to be caused by thin layers of gas at the BGHS (Singh et al., 1993). On the Hikurangi Margin, thick FGZs are evident elsewhere in seismic lines (Text S7 in Supporting Information S1). A ∼250 m thick FGZ beneath hydrates was studied during scientific drilling on the Blake Ridge, US Atlantic Margin (Holbrook et al., 1996; Paull et al., 2000). Although no evidence for hydrate was found in the FGZ there, we speculate that other thick FGZs globally may host dissociating hydrate.

A widespread presence of hydrate in FGZs would increase the estimated amount of carbon bound in hydrate globally. The density of carbon in hydrate, however, is similar to that in free gas at these depths (Boswell & Collet, 2011) (Text S8 in Supporting Information S1). If counting gas trapped by capillary forces toward the carbon buffer of hydrate systems, the difference between the pore-space saturation of hydrate and that of immobile free gas needs to be considered. We measured 40%–60% hydrate saturation at several levels in the FGZ whereas gas mobility increases significantly already at saturations <20% (Jang & Santamarina, 2014). Dissociating hydrates in the FGZ may therefore bind more carbon than immobile free gas but their effect on carbon budgets of hydrate systems is difficult to constrain.

In summary, at Site U1519, we observe strong evidence for hydrate within the FGZ down to ∼60 m below the regional BSR. Our findings suggest gas hydrate is in the process of dissociation that is taking place over thousands of years.

Data Availability Statement

Logging data are archived at the Lamont–Doherty Earth Observatory's Division of Marine and Large Programs (https://mlp.ldeo.columbia.edu/data/iodp-usio/exp372/U1519A/). Results from coring are archived at the International Ocean Discovery Program (https://web.iodp.tamu.edu/OVERVIEW/?&exp=372&site=U1519). Line 05CM-04 raw and industry-processed data are available from the New Zealand Petroleum and Minerals' Geodata database (https://geodata.nzpam.govt.nz/, Petroleum Report 05CM:PR3136). Codes and data are accessible as a tar archive at Zenodo (I. Pecher, 2025).

Acknowledgments
This research used samples and/or data provided by the International Ocean Discovery Program (IODP). We thank IODP, Texas A&M University, Schlumberger Drilling and Measurements, the crew of the JOIDES Resolution, and the Expedition 375 and 372 science parties, as well as two anonymous reviewers for their constructive comments. I. Pecher acknowledges funding by the New Zealand Ministry of Business, Innovation, and Employment (MBIE, Contract C05X1708), A. Cook by the National Science Foundation (NSF, Award #1752882), E. Solomon by NSF (#1753617), X. Wang by the National Natural Science Foundation of China (41976077), P. Barnes by MBIE (CO5X1605) as well as NIWA SSIF core funding (COPR), and K. Heeschen by the German IODP Office (Deutsche Forschungsgemeinschaft).

References

Bangs, N. L. B., Sawyer, D. S., & Golovchenko, X. (1993). Free gas at the base of the gas hydrate zone in the vicinity of the Chile triple junction. *Geology*, *21*(10), 905–908. https://doi.org/10.1130/0091-7613(1993)021<0905:fgatbo>2.3.co;2

Barnes, P. M., Wallace, L. M., Saffer, D. M., Pecher, I. A., Petronotis, K. E., LeVay, L. J., et al. (2019). Site U1519. In L. M. Wallace, D. M. Saffer, P. M. Barnes, I. A. Pecher, K. E. Petronotis, L. J. LeVay, & Expedition 372/375 Scientists (Eds.), *Proceedings of the International Ocean Discovery Program*, *Hikurangi Subduction Margin coring, logging, and observatories* (Vol. 372B/375). International Ocean Discovery Program. https://doi.org/10.14379/iodp.proc.372b375.104.2019

Biastoch, A., Treude, T., Rüpke, L. H., Riebesell, U., Roth, C., Burwicz, E. B., et al. (2011). Rising Arctic Ocean temperatures cause gas hydrate destabilization and ocean acidification. *Geophysical Research Letters*, *38*(8), L08602. https://doi.org/10.1029/2011GL047222

Boetius, A., & Wenzhöfer, F. (2013). Seafloor oxygen consumption fuelled by methane from cold seeps. *Nature Geoscience*, *6*(9), 725–734. https://doi.org/10.1038/ngeo1926

Boswell, R., & Collet, T. (2011). Current perspectives on gas hydrate resources. *Energy & Environment*, *4*, 1206–1215. https://doi.org/10.1039/c0ee00203h

Buffett, B. A., & Archer, D. (2004). Global inventory of methane clathrate: Sensitivity to changes in the deep ocean. *Earth and Planetary Science Letters*, *227*(3–4), 185–199. https://doi.org/10.1016/j.epsl.2004.09.005

Clark, P. U., Shakun, J. D., Baker, P. A., Bartlein, P. J., Brewer, S., Brook, E., et al. (2012). Global climate evolution during the last deglaciation. *Proceedings of the National Academy of Sciences*, *109*(19), E1134–E1142. https://doi.org/10.1073/pnas.1116619109

Cook, A. E., & Waite, W. F. (2018). Archie's saturation exponent for natural gas hydrate in coarse-grained reservoirs. *Journal of Geophysical Research: Solid Earth*, *123*(3), 2069–2089. https://doi.org/10.1002/2017JB015138

Crundwell, M. P., & Woodhouse, A. (2022). Biostratigraphically constrained chronologies for Quaternary sequences from the Hikurangi margin of north-eastern Zealandia. *New Zealand Journal of Geology and Geophysics*, *67*(3), 1–21. https://doi.org/10.1080/00288306.2022.2101481

Crutchley, G., Fraser, D., Pecher, I., Gorman, A., Maslen, G., & Henrys, S. (2015). Natural gas injection into gas hydrate bearing sediments on the southern Hikurangi margin of New Zealand. *Journal of Geophysical Research*, *120*(2), 725–743. https://doi.org/10.1002/2014JB011503

DeMets, C., Gordon, R. G., Argus, D. F., & Steins, S. (1990). Current plate motions. *Geophysical Journal International*, *101*(2), 425–478. https://doi.org/10.1111/j.1365-246x.1990.tb06579.x

Dickens, G. R. (2003). Rethinking the global carbon cycle with a large, dynamic and microbially mediated gas hydrate capacitor. *Earth and Planetary Science Letters*, *213*(3–4), 169–183. https://doi.org/10.1016/S0012-821X(03)00325-X

Ellis, D. V., & Singer, J. M. (2007). *Well logging for earth Scientists*. Springer.

Fowler, C. M. R. (2005). *The solid Earth* (2nd ed.). Cambridge University Press.

Goto, S., Matsubayashi, O., & Nagakubo, S. (2016). Simulation of gas hydrate dissociation caused by repeated tectonic uplift events. *Journal of Geophysical Research: Solid Earth*, *121*(5), 3200–3219. https://doi.org/10.1002/2015JB012711

Han, S., Bangs, N. L., Hornbach, M. J., Pecher, I. A., Tobin, H. J., & Silver, E. A. (2021). The many double BSRs across the Northern Hikurangi margin and their implications for subduction processes. *Earth and Planetary Science Letters*, *558*, 116743. https://doi.org/10.1016/j.epsl.2021.116743

Helgerud, M. B., Dvorkin, J., Nur, A., Sakai, A., & Collett, T. (1999). Elastic-wave velocity in marine sediments with gas hydrates: Effective medium modeling. *Geophysical Research Letters*, *26*(13), 2021–2024. https://doi.org/10.1029/1999gl900421

Helgerud, M. B., Waite, W. F., Kirby, S. H., & Nur, A. (2009). Elastic wave speeds and moduli in polycrystalline ice Ih, sI methane hydrate, and sII methane-ethane hydrate. *Journal of Geophysical Research*, *114*(B2), B02212. https://doi.org/10.1029/2008JB006132

Hill, R. (1952). The elastic behavior of crystalline aggregate. *Proceedings of the Physical Society, London*, *A65*, 349–354.

Holbrook, W. S., Hoskins, H., Wood, W. T., Stephen, R. A., & Lizarralde, D., & Leg 164 Scientific Party. (1996). Methane hydrate and free gas on the Blake Ridge from vertical seismic profiling. *Science*, *273*(5283), 1840–1843. https://doi.org/10.1126/science.273.5283.1840

Jang, J., & Santamarina, J. C. (2014). Evolution of gas saturation and relative permeability during gas production from hydrate-bearing sediments: Gas invasion vs. gas nucleation. *Journal of Geophysical Research: Solid Earth*, *119*(1), 116–126. https://doi.org/10.1002/2013JB010480

Kang, D., Zhang, Z., Liang, J., Kuang, Z., Lu, C., Kou, B., et al. (2020). Fine-grained gas hydrate reservoir properties estimated from well logs and lab measurements at the Shenhu gas hydrate production test site, the northern slope of the South China Sea. *Marine and Petroleum Geology*, *122*, 104676. https://doi.org/10.1016/j.marpetgeo.2020.104676

Kastner, M., Elderfield, H., & Martin, J. B. (1991). Fluids in convergent margins: What do we know about their composition, origin, role in diagenesis and importance for oceanic chemical fluxes? *Philosophical Transactions of the Royal Society of London - A*, *335*, 243–259.

Kennett, J. P., Cannariato, K. G., Hendy, I. L., & Behl, R. J. (2000). Carbon isotopic evidence for methane hydrate instability during quaternary interstadials. *Science*, *288*(5463), 128–133. https://doi.org/10.1126/science.288.5463.128

Kroeger, K., Kroeger, K., Plaza-Faverola, A., Barnes, P. M., & Pecher, I. A. (2015). Thermal evolution of the New Zealand Hikurangi subduction margin: Impact on natural gas generation and methane hydrate formation - A model study. *Marine and Petroleum Geology*. JMPG-D-14-00270R2

Lambeck, K., Rouby, H., Purcell, A., Sun, Y., & Sambridge, M. (2014). Sea level and global ice volumes from the Last Glacial Maximum to the Holocene. *Proceedings of the National Academy of Sciences of the United States of America*, *111*(43), 15296–15303. https://doi.org/10.1073/pnas.1411762111

Lee, M. W. (2002). Biot-Gassmann theory for velocities of gas hydrate-bearing sediments. *Geophysics*, *67*(6), 1711–1719. https://doi.org/10.1190/1.1527072

Lee, M. W. (2008). *Comparison of the modified Biot–Gassmann theory and the Kuster–Toksoez theory in predicting elastic velocities of sediments (USGS Sci. Invest. Rep.)* (p. 21). U.S. Geological Survey.

Lee, M. W., & Collet, T. S. (2005). Assessment of gas hydrate concentrations estimated from sonic logs in the JAPEX/JNOC/GSC et al. Mallik 5L-38 gas hydrate research production well. In S. R. Dallimore & T. S. Collet (Eds.), *Scientific results from the Mallik 2002 gas hydrate production research well program, Mackenzie Delta, Northwest Territories, Canada* (p. 10).

Liu, X., & Flemings, P. B. (2007). Dynamic multiphase flow model of hydrate formation in marine sediments. *Journal of Geophysical Research*, *112*(B3), B03101. https://doi.org/10.1029/2005JB004227

Malinverno, A., Kastner, M., Torres, M. E., & Wortmann, U. G. (2008). Gas hydrate occurrence from pore water chlorinity and downhole logs in a transect across the northern Cascadia margin (Integrated Ocean Drilling Program Expedition 311). *Journal of Geophysical Research*, *113*(B8), B08103. https://doi.org/10.1029/2008JB005702

Maslin, M., Owen, M., Betts, R., Day, S., Dunkley Jones, T., & Ridgwell, A. (2010). Gas hydrates: Past and future geohazard? *Philosophical Transactions of the Royal Society A*, *368*(1919), 2369–2393. https://doi.org/10.1098/rsta.2010.0065

Mavko, G., Mukerji, T., & Dvorkin, J. (2020). *The rock physics handbook*. Cambridge University Press.

Milkov, A. V., Xu, W., Dickens, G. R., Borowski, W. S., Claypool, G. E., & Borowski, W. S. (2003). In situ methane concentrations at Hydrate Ridge, offshore Oregon: New constraints on the global gas hydrate inventory from an active margin. *Geology*, *31*(10), 833–836. https://doi.org/10.1130/G19689.1

Mountjoy, J. J., Pecher, I., Henrys, S., Crutchley, G., Barnes, P. M., & Plaza-Faverola, A. (2014). Shallow methane hydrate system controls ongoing, downslope sediment transport in a low-velocity active submarine landslide complex, Hikurangi Margin, New Zealand. *Geochemistry, Geophysics, Geosystems*, *15*(11), 4137–4156. https://doi.org/10.1002/2014GC005379

Multiwave. (2005). *05CM 2D seismic survey, offshore east coast - North Island (PR3136)* (p. 280). Ministry of Economic Development.

Navalpakam, R. S., Pecher, I. A., & Stern, T. (2012). Weak and segmented bottom simulating reflections on the Hikurangi Margin, New Zealand—Implications for gas hydrate reservoir rocks. *Journal of Petroleum Science & Engineering*, *88–89*, 29–40. https://doi.org/10.1016/j.petrol.2012.01.008

Nole, M., Daigle, H., Cook, A. E., Malinverno, A., & Flemings, P. B. (2018). Burial-driven methane recycling in marine gas hydrate systems. *Earth and Planetary Science Letters*, *499*, 197–204. https://doi.org/10.1016/j.epsl.2018.07.036

Oluwunmi, P., Pecher, I., Archer, R., Reagan, M., & Moridis, G. (2022). The response of gas hydrates to tectonic uplift. *Transport in Porous Media*, *144*(3), 739–758. https://doi.org/10.1007/s11242-022-01837-w

Pabst, W., & Gregorová, E. V. A. (2013). Elastic properties of silica polymorphs–A review. *Ceramics-Silikáty*, *57*(3), 167–184.

Paganoni, M., Cartwright, J. A., Foschi, M., Shipp, R. C., & Van Rensbergen, P. (2016). Structure II gas hydrates found below the bottom simulating reflector. *Geophysical Research Letters*, *43*(11), 5696–5706. https://doi.org/10.1002/2016GL069452

Paull, C. K., Matsumoto, R., Wallace, P. J., & Dillon, W. P. (2000). *Proc. ODP, Sci. Results* (Vol. 164). Ocean Drilling Program.

Paull, C. K., Ussler, W., & Borowski, W. S. (1994). Sources of biogenice methane to form marine gas hydrates. In E. D. Sloan, J. Happle, & M. A. Hnatow (Eds.), *International conference on natural gas hydrates* (Vol. 715, pp. 393–409). Plenum Press.

Pecher, I. (2025). *Codes and data for Pecher et al., dissociating gas hydrate beneath the hydrate stability zone, submitted to Geophys. Res. Lett. In Geophysical Research Letters. [Collection]*. Zenodo. https://doi.org/10.5281/zenodo.12698211

Pecher, I. A., & Henrys, S. A. (2003). *Potential gas reserves in gas hydrate sweet spots on the Hikurangi Margin, New Zealand (Science Report No. 2003/23)* (p. 32). Lower Hutt: Institute of Geological and Nuclear Sciences.

Pecher, I. A., Minshull, T. A., Singh, S. C., & von Huene, R. (1996). Velocity structure of a bottom simulating reflector offshore Peru: Results from full waveform inversion. *Earth and Planetary Science Letters*, *139*(3–4), 459–469. https://doi.org/10.1016/0012-821x(95)00242-5

Pecher, I. A., Villinger, H., Kaul, N., Crutchley, G. J., Mountjoy, J. J., Huhn, K., et al. (2017). A fluid pulse on the Hikurangi Subduction Margin: Evidence from a heat flux transect across the upper limit of gas hydrate stability. *Geophysical Research Letters*, *44*(24), 12385–12395. https://doi.org/10.1002/2017GL076368

Portnov, A., Cook, A. E., Sawyer, D. E., Yang, C., Hillman, J. I. T., & Waite, W. F. (2019). Clustered BSRs: Evidence for gas hydrate-bearing turbidite complexes in folded regions, example from the Perdido Fold Belt, northern Gulf of Mexico. *Earth and Planetary Science Letters*, *528*, 115843. https://doi.org/10.1016/j.epsl.2019.115843

Qian, J., Wang, X., Collett, T. S., Guo, Y., Kang, D., & Jin, J. (2018). Downhole log evidence for the coexistence of structure II gas hydrate and free gas below the bottom simulating reflector in the South China Sea. *Marine and Petroleum Geology*, *98*, 662–674. https://doi.org/10.1016/j.marpetgeo.2018.09.024

Qin, X., Lu, J., Lu, H., Qiu, H., Liang, J., Kang, D., et al. (2020). Coexistence of natural gas hydrate, free gas and water in the gas hydrate system in the Shenhu Area, South China Sea. *China Geology*, *3*(2), 210–220. https://doi.org/10.31035/cg2020038

Ruppel, C. D. (2011). Methane hydrates and contemporary climate change. *Nature Education Knowledge*, *3*(10), 29.

Saumya, S., Narasimhan, B., Singh, J., Yamamoto, H., Vij, J., Sakiyama, N., & Kumar, P. (2019). Acquisition of logging-while-drilling (LWD) multipole acoustic log data during the India national gas hydrate program (NGHP) expedition 02. *Marine and Petroleum Geology*, *108*, 562–569. https://doi.org/10.1016/j.marpetgeo.2018.10.011

Schoen, J. H. (1996). *Physical properties of rocks* (Vol. 18). Elsevier Science.

Shkvorets, I. (2025). Salinometry. Retrieved from https://salinometry.com/ctd-salinity-calculator/

Singh, S. C., Minshull, T. A., & Spence, G. D. (1993). Velocity structure of a gas hydrate reflector. *Science*, *260*(5105), 204–207. https://doi.org/10.1126/science.260.5105.204

Sloan, E. D., & Koh, C. A. (2007). *Clathrate hydrates of natural gases* (3rd ed.). Marcel Bekker.

Tréhu, A., Flemings, P. B., Bangs, N. L., Chevallier, J., Gràcia, E., Johnson, J. E., et al. (2004). Feeding methane vents and gas hydrate deposits at south Hydrate Ridge. *Geophysical Research Letters*, *31*(23), L23310. https://doi.org/10.1029/2004GL021286

Tréhu, A. M., & Flueh, E. R. (2001). Estimating the thickness of the free gas zone beneath Hydrate Ridge, Oregon continental margin, from seismic velocities and attenuation. *Journal of Geophysical Research*, *106*(B2), 2035–2045. https://doi.org/10.1029/2000JB900390

Ussler, W. I., & Paull, C. K. (1995). Effects of ion-exclusion and isotopic fractionation on pore-water geochemistry during gas hydrate formation and decomposition. *Geo-Marine Letters*, *15*(1), 37–44. https://doi.org/10.1007/BF01204496

Waelbroeck, C., Labeyrie, L., Michel, E., Duplessy, J.-C., Mcmanus, J. F., Lambeck, K., et al. (2002). Sea-level and deep water temperature changes derived from benthic foraminifera isotopic records. *Quaternary Science Reviews*, *21*(1–3), 295–305. https://doi.org/10.1016/s0277-3791(01)00101-9

Wallace, L. M., Saffer, D. M., Barnes, P. M., Pecher, I. A., Petronotis, K. E., & LeVay, L. J., & Expedition 372/375 Scientists. (2019). *Hikurangi Subduction Margin coring, logging, and observatories* (Vol. 372B/375). International Ocean Discovery Program.

Wallmann, K., Pinero, E., Burwicz, E., Haeckel, M., Hensen, C., Dale, A., & Ruepke, L. (2012). The global inventory of methane hydrate in marine sediments: A theoretical approach. *Energies*, *5*(7), 2449–2498. https://doi.org/10.3390/en5072449

You, K., & Flemings, P. (2021). Methane hydrate formation and evolution during sedimentation. *Journal of Geophysical Research: Solid Earth*, *126*(4), e2020JB021235. https://doi.org/10.1029/2020jb021235

References From the Supporting Information

Aylward, I., Solomon, E. A., Torres, M. E., Whorley, T. L., Harris, R. N., Hillman, J., & Philip, B. (2020). *Geochemical constraints on the Hikurangi margin hydrogeologic system – Results from the SAFFRONZ Expedition*. Presented at the AGU Fall Meeting.

Aylward, I., Solomon, E. A., Whorley, T. L., Miller, R., Hillman, J., Seabrook, S., et al. (2023). *The evolution of fluid flow throughout the slow slip cycle: Testing the hydrologic response to SSEs at the Hikurangi subduction zone*. Presented at the AGU Fall Meeting.

Barnes, J. D., Cullen, J., Barker, S., Agostini, S., Penniston-Dorland, S., Lassiter, J. C., et al. (2019). The role of the upper plate in controlling fluid-mobile element (Cl, Li, B) cycling through subduction zones: Hikurangi forearc, New Zealand. *Geosphere*, *15*(3), 642–658. https://doi.org/10.1130/ges02057.1

Hensen, C., Wallmann, K., Schmidt, M., Ranero, C. R., & Suess, E. (2004). Fluid expulsion related to mud extrusion off Costa Rica—A window to the subducting slab. *Geology*, *32*(3), 201–204. https://doi.org/10.1130/g20119.1

Kastner, M., Solomon, E. A., Harris, R. N., & Torres, M. E. (2014). Fluid origins, thermal regimes, and fluid and solute fluxes in the forearc of subduction zones. In *Developments in marine geology* (Vol. 7, pp. 671–733). Elsevier. https://doi.org/10.1016/b978-0-444-62617-2.00022-0

Luo, M., Yu, M., Torres, M. E., Solomon, E. A., Gieskes, J., You, C.-F., et al. (2024). Volcanic ash alteration triggers active sedimentary lithium cycling: Insights from lithium isotopic compositions of pore fluids and sediments in the Hikurangi subduction zone. *Earth and Planetary Science Letters*, *642*, 118854. https://doi.org/10.1016/j.epsl.2024.118854

Manheim, F. T., & Waterman, L. S. (1974). *Diffusimetry (diffusion constant estimation) on sediment cores by resistivity probe* (Vol. 22, pp. 663–670). Initial Reports of the Deep Sea Drilling Project.

Martin, J. B., Kastner, M., Henry, P., Le Pichon, X., & Lallement, S. (1996). Chemical and isotopic evidence for sources of fluids in a mud volcano field seaward of the Barbados accretionary wedge. *Journal of Geophysical Research*, *101*(B9), 20325–20345. https://doi.org/10.1029/96jb00140

Mottl, M. J., Wheat, C. G., Fryer, P., Gharib, J., & Martin, J. B. (2004). Chemistry of springs across the Mariana forearc shows progressive devolatilization of the subducting plate. *Geochimica et Cosmochimica Acta*, *68*(23), 4915–4933. https://doi.org/10.1016/j.gca.2004.05.037

Philip, B. T., Solomon, E. A., Kelley, D. S., Tréhu, A. M., Whorley, T. L., Roland, E., et al. (2023). Fluid sources and overpressures within the central Cascadia Subduction Zone revealed by a warm, high-flux seafloor seep. *Science Advances*, *9*(4), eadd6688. https://doi.org/10.1126/sciadv.add6688

Poisson, A., & Papaud, A. (1983). Diffusion coefficients of major ions in seawater. *Marine Chemistry*, *13*(4), 265–280. https://doi.org/10.1016/0304-4203(83)90002-6

Ranero, C. R., Grevemeyer, I., Sahling, H., Barckhausen, U., Hensen, C., Wallmann, K., et al. (2008). Hydrogeological system of erosional convergent margins and its influence on tectonics and interplate seismogenesis. *Geochemistry, Geophysics, Geosystems*, *9*(3), Q03S04. https://doi.org/10.1029/2007gc001679

Screaton, E. J., Wuthrich, D. R., & Dreiss, S. J. (1990). Permeabilities, fluid pressure, and flow rates in the Barbados ridge complex. *Journal of Geophysical Research*, *100*, 8897–9007.

Winsauer, W. O., Shearin, H. M., Masson, P. H., & Williams, M. (1925). Resistivity of brine-saturated sands in relation to pore geometry. *AAPG Bulletin*, *36*, 253–277. https://doi.org/10.1306/3D9343F4-16B1-11D7-8645000102C1865D

You, C.-F., Castillo, P., Gieskes, J., Chan, L., & Spivack, A. (1996). Trace element behavior in hydrothermal experiments: Implications for fluid processes at shallow depths in subduction zones. *Earth and Planetary Science Letters*, *140*(1–4), 41–52. https://doi.org/10.1016/0012-821x(96)00049-0